Wilting Deformation of Leaves Using Cell Dynamics and Time-Varying External Forces

Anonymous cvm submission

Paper ID 337

Abstract

In this article, we proposed an algorithm to simulate the withered deformation with wrinkle and curl of plant leaves due to the dehydration, basing the cell swelling force and time-varying external force. Firstly, we proposed the leaf boundary expansion algorithm to locate the feature points on the tips of the veins, and calculated the discrete geodesic paths to construct the primary veins. Secondly, we defined a novel mass-spring system by the cell dynamics, and the non-uniform mass distribution, to accelerate the movement of the boundary cells. Thirdly, we defined the cell swelling force on the osmosis, to generate the wrinkle deformation by adjusting the dehydration and the cell swelling force. Fourthly, we defined the system's time-varying external forces on the feature points of the vein, to generate the curl deformation by adjusting the initial values of the external forces and the multiple iterative parameters. Finally, we used the implicit midpoint method to solve the equation of motion iteratively to achieve deformation simulation. The experimental results show that our algorithm can simulate the wrinkle and curl deformation caused by dehydration and withering of leaves with higher authenticity.

1. Introduction

The geometric modeling of plant leaves, and the simulation of leaf geometry deformation due to changes in ambient temperature and humidity, both are in strong demand in a variety of fields recently, e.g., in film and animation industry, video games, education, scientific research, especially in the agricultural informatization field [1, 2]. In this article, out fruitful work has resulted in a solution of simulating the wrinkle and curl deformation of leaves during the dehydration process.

Leaf veins are the mechanical support skeleton of leaves, which changes shape as the leaf curls and wrinkles. The correlative research work at home and abroad can be divided into interactive method [3], image deformation method [4], and biological drive method [5], etc. However, most of the previous studies of wilting deformation have not dealt with the mechanical supporting effect of veins, which leads to the of lack mechanical structural principles in their leaf models. As a result, the results of the simulations are not good enough and the computational efficiency is comparatively low.

One of the aims of this research has therefore been to improve the simulation authenticity of leaves curl and wrinkle deformation. In this article, we construct the primary veins of plant leaf by using the discrete geodesic path, and introduce a boundary expansion method to construct the tip feature points of the veins in a 3D leaf mesh model to achieve our goals.

Furthermore, Even though previous studies have made great progress in this field, most of them ignored the cell swelling force within the plant itself and the influence of external factors, which are violate the principle of the cell dynamics [6]. To solve these problems, first, we construct a leaf mass-spring structure model according to the principle of the cell dynamics; then we introduce a non-uniform mass distribution to adjust the motion state of the cells as plasmids in different regions to increase the deformation acceleration of cells in the boundary region; moreover, we introduce permeation effect of cells to define the cell swelling force. The force can be controlled by adjusting the dehydration rate to generate the wrinkle deformation; finally, system's time-varying external forces are introduced at the feature points of the vein tips to generate the curl deformation by adjusting the initial value of the time-varying external forces and the iterative parameters.

The main contributions and innovations of our work can be summarized as follows:

- A leaf boundary expansion method was proposed to locate the feature points on the tips of the veins.
- The primary veins are constructed by calculating the discrete geodesic paths.
- A non-uniform distribution of leaf cell mass is defined to optimize the deformation effect.
- Wrinkle deformation is effectively controlled by introducing the cell expansion force.
- Curl deformation is adjusted by introducing the system's time-varying external forces.

2. Related work

Changes in ambient temperature and humidity affect the water content of leaves, which in turn may lead to cell dehydration and cause the wilting deformation of the leaf wrinkles and curls. In this article, our simulation of the leaf wilting process can be divided into two parts: vein modeling and leaf cell mechanics modeling.

In terms of the veins modeling, in 2010, Qin and Xiao [3] published a paper in which they proposed an interactive modeling method that uses the user-interactive modification to create the 3D shape of leaf veins, which is highly dependent on the attributes provided by the users. However, this method has the disadvantage of ignoring the physiological characteristics of plants and the lack of biological and physical principles of the deformation process.

Recently, many studies have implemented more realistic simulations of leaf veins in 2D, e.g., in 2016, a contour-based leaf vein modeling method proposed by Kim and Kim [4] uses binary images of leaves to construct veins, and in 2017, biological driving methods (Runions et al. and Alsweis et al. [5, 7]) implemented the modeling and visualization of the leaf veins growing process. However, these simulations are only in the 2D plane and the latter two methods generated leaf edges are difficult to control.

In terms of the leaf deformation simulation, several attempts have been made to improve the efficiency and quality of deformation simulations. In 2009, A physics-based two-layer leaf model proposed by Chi et al. [8] successfully simulates the deformation of leaves in autumn, which upper layer represents the leaf sarcomeres with higher shrinkage rates, and the lower layer represents the vein cells that are more resistant to shrinkage and more rigid. Two layers are connected to maintain the mechanical stability of leaves. A mass-spring system is constructed between those two layers to simulate the different kinetics behaviors between the mesophyll cells and vein cells. As a result, the two layers influence each other to jointly determine the deformed shape of leaves. The advantage of this method is that it better exploits biological features, but the computational complexity of this method is high. Similarly, in 2013, Jeong et al. [11] have proposed a principle of the double-layered mass-spring model. The difference is that in Jeong's method, both the vein and leaf flesh models are double-layered, and a water penetration model is constructed as well. As a result, this method can adjust the degree of curl according to the differences in water content between the various parts of the leaf, thus a more realistic simulation effect can be obtained by the method. However, the veins and mesophyll are bi-layered, which does not correspond to the objective physiological structure of the leaf. Besides, the method has more masses and springs, which leads to the high computational complexity of the algorithm. Another method was proposed by Chi et al. [9] in 2009 to simulate the wilting and aging process of leaves based on the large-scale leaf sampling, however, the computational efficiency of this method is relatively low.

In order to simplify the deformation design process and optimize the deformation simulation results, in 2015, Wei et al. [12] proposed a half-process and half-physical leaf deformation algorithm. The method first sets the target state of the veins, and then constructs the intermediate state sequence of the vein deformation by interpolating between the initial state and the target state. The mesophyll is deformed by the elastic force of the veins, which improve the coordination between the spring coefficient and deformation. However, the disadvantage is that the veins model needs to be constructed manually, which is not suitable for large-scale leaf modeling.

A novel method was proposed by Xiao and Chen [10] in 2011. This method takes the contraction strain field as the driving force of the wrinkling morphology, and controls the degree of leaf deformation by adjusting parameters. However, this method doesn't consider the role of veins, ignores structural analysis, and lacks biological principles.

Recently, in 2018, Liu et al. [13] proposed a method, which is based on the feature that the wrinkle deformation is more obvious and the curl deformation is weaker during the initial stage of dehydration. When the water content drops to a critical value, the shrinkage difference along the boundary to the veins defines the curl deformation, which provides some inspiration for the leaf deformation algorithm in our article.

In view of all that has been mentioned so far, one may suppose that the construction of a realistic and efficient leaf vein model and the provision of an accurate and efficient deformation algorithm play a crucial role in the simulation of leaf wilt deformation.

In the section 3 of this article, we define the feature points of the veins by using a leaf boundary expansion algorithm, and calculate the discrete geodesic paths to construct the primary veins; In section 4, we define the mass-spring system for cells, construct a non-uniform mass distribution, give the calculation method of water content under dehydration, define the cell swelling force and time-varying external forces; Section 5 gives some experimental results and analysis; Section 6 summarizes the article. Figure 1 is the flow chart of the algorithm.

3. Construct veins

In this section, in order to more accurately and efficiently generate the primary leaf veins, we propose a boundary expansion algorithm in the process of generating the primary leaf veins. The process is divided into three steps. We first construct a 3D mesh model of the leaves by the half-edge structure. Then, we use multi-dimensional scaling (MDS) to map the 3D leaf model into 2D space [14]. Once in 2D space, our boundary expansion algorithm is able to locate the local extreme points on the leaf boundary.

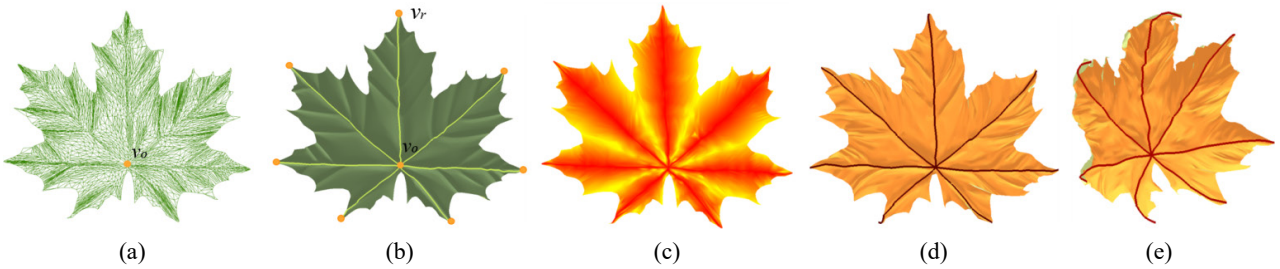

Fig. 1. Algorithm flow chart. In this article, we construct the 3D leaf model (a), locate the primary leaf veins (b), propose a non-uniform distribution of mass (c) to simulate the wrinkle deformation effect (d) and curl deformation effect (e) of plant leaf.

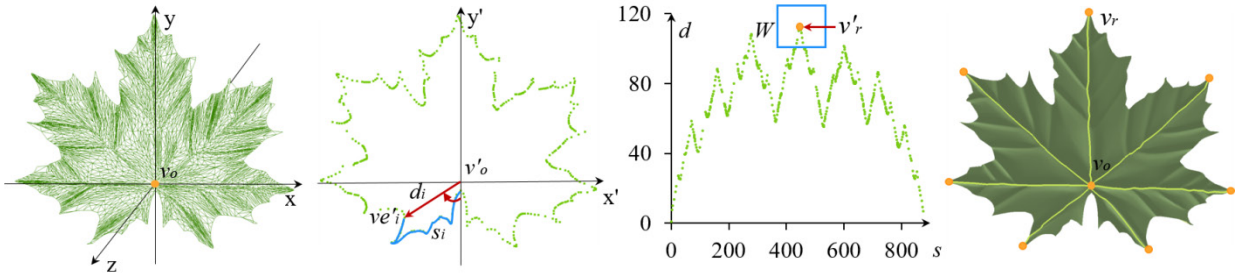

Fig. 2. The pipeline of constructing the primary veins. For a 3D leaf model (a), get the 2D boundary points (b) and form the boundary expansion coordinate (c) to construct the primary veins (d).

We shall take these points as the feature points of vein tips. Finally, we can use the obtained feature points in combination with discrete geodetic paths [15] to construct the primary leaf veins.

Let $G=\{V, E, F\}$ indicates the 3D mesh model of the leaf ,where $V=\{v_1, v_2,\ldots, v_n\}$ denotes the vertices set and $E=\{<e_{ij}, e_{ji}>, v_i, v_j \in V\}$is the set of symmetrical directed half-edges. When e_{ij} takes a non-zero value, it means that there exists a directed half-edge from vertex v_i pointing to vertex v_j. If half-edge e_{ij} has no opposite half-edge e_{ji}, i.e., e_{ji} is on the boundary. $V_E=\{ve_1, ve_2,\ldots, ve_{ne}\}$ denotes the set of such half-edges' endpoints, where ne is the number of boundary vertices. $F=\{f_1, f_2,\ldots, f_m\}$ is the set of the triangular faces of the leaf model.

$\boldsymbol{D} \in \mathrm{R}^{n\times n}$ is the distance matrix between the different vertices of G, whose element gd_{ij} indicates the discrete geodesic distance between the vertex v_i and v_j. Using MDS to map the mesh model G from 3D space to 2D, the results are denoted by G', the vertices set of G' is $\{v_1', v_2', \ldots, v_n'\}$. Then the mapping process between the model G and G' can be transferred to solve the following optimization [16]:

$$\min_{v_1',\ldots,v_n'} \sum_{i<j} \left(\left\|v_i' - v_j'\right\| - gd_{ij}\right)^2, \; i,j = 1,2,\ldots,n$$

For any vertex ve'_i at the boundary of the 2D mesh model G', d_i indicates the Euclidean distance between ve'_i and the petiole point v'_o (see Figur 2(b)). Calculating the cumulative length s_i of the boundary polyline from the boundary vertex ve'_i to the petiole point v'_o along the boundary of G' in a clockwise direction. Taking the cumulative length s as the horizontal axis, d as the vertical axis and the (s_i, d_i) representing the coordinates of the boundary point ve'_i, the coordinate system of boundary expansion is drawn as shown in Figure 2(c) [17].

A sliding window W is defined with width k along the coordinate curve of the boundary vertices. In the window W, if there exists a boundary vertex v'_r with boundary vertices on both sides, satisfying the following conditions: $\exists\, r = i + k/2$, $d_i < \ldots < d_{r-1} < d_r < d_{r+1} < \ldots < d_{i+k}$, that boundary point v_r is defined as a feature point of the veins of model G in the 3D space.

In this article, we take the discrete measure path between the petiole point v_0 and the feature point v_r of each vein on the boundary as the primary veins of the leaf model G. The primary veins and the feature points of veins shall affect the non-uniform distribution of the initial mass of cells. And the feature points of veins are also the action points of system's time-varying external forces

4. The wrinkle and curl deformation

In this section, in order to achieve an accurate simulation of wrinkle and curl deformation during leaf wilting process, we first define a plant leaf as a system of cells regarded as particles connected by springs according to cell dynamics [18] and mass-spring system [19]. Then we construct the mass-spring system according to the elastic force and damping force of the cells, generate the swelling force of leaves from the permeation effect of cells, and define the continuous time-varying external force at the feature points

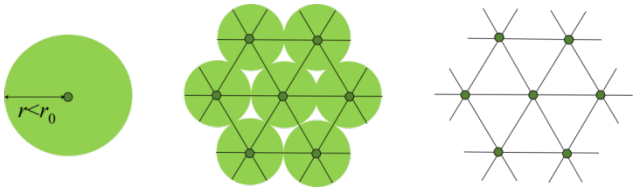

(a) (b) (c)

Fig. 3. Intercellular mass-spring structure. From left to right, it shows a single model of cell (a); a set of cell models (b); a simplified mass point-spring model (c).

v_r of the veins. Finally, we combine all the above forces to implement the deformation simulation of leaves.

4.1. Mass-spring system

The cell dynamics-based model of plant leaf cells and its mass-spring system are shown in Figure 3. Figure 3(a) shows a single cell filled with cell sap, where r_0 and r represent the cell radius in the liquid-filled state of cells and the cell radius at shrinkage from dehydration, respectively. Figure 3(b) shows the mesophyll tissue formed by tightly arranged multiple cells, with plasmodesmata connected between the adjacent cells. Regarding cells as particles and plasmodesmata as springs, the mass-spring system corresponding to the mesophyll tissue of the multicellular leaf in Figure 3(b) is shown in Figure 3(c).

In this article, the vertices set V of the 3D mesh model $G=\{V, E, F\}$ is used as the particles of the mass-spring system, and the edge set E represents the springs which connecting the particles. The mass-spring system of G is shown in Figure 4. Figure 4(a) shows the distribution model of the spring. In the one-ring neighborhood of the particle v_i, the number of particles connecting to v_i is m, and m adjacent triangular patches are formed in the neighborhood. In the mass-spring system, v_i is stretched or squeezed by m particles in the one-ring neighborhood, the stress analysis of v_i is shown in Figure 4(b).

4.2. Non-uniform distribution of mass

To better simulate the forces on each cell, in this article, we set up a non-uniform distribution of the initial mass of leaf cells corresponding to each particle in the mass-spring system. The mass m_i of a cell v_i is composed of the water content w_i and cytosol s_i. The initial mass of each mesophyll cell is obtained by the interpolation of the distance from the cell to the nearest leaf vein:

$$m_i^0=m_{min}\left(1-\left(1-\frac{gd_i}{gd_{max}}\right)^{\tau}\right)+m_{max}\left(1-\frac{gd_i}{gd_{max}}\right)^{\tau}$$

where $\tau \in [0,1]$ indicates the coefficient of mass distribution, when $\tau=1$, the mass of cells decreases linearly

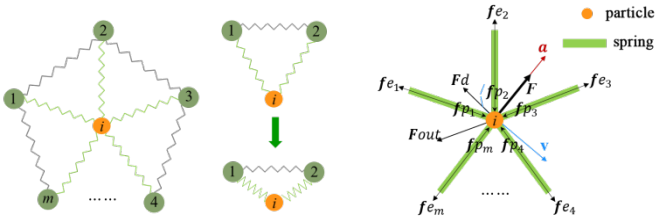

(a) (b)

Fig. 4. Mass-spring model combined with cell mechanics. From left to right, it shows the adjacency deformation of particle v_i (a); the stress and motion state of particle v_i (b).

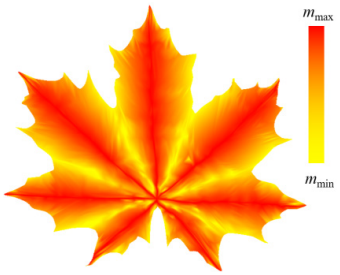

Fig. 5. Non-uniform distribution of particle cell mass

from vein cells to boundary cells, and when $\tau \neq 1$, the mass of cells decreases nonlinearly. m_{min} and m_{max} are the minimum and maximum values for the mass of the leaf vein cells. For each vein cell, there are multiple neighboring mesophyll cells surrounding it. gd_{max} is the maximum value of their distance from that vein cell. Figure 5 shows the non-uniform distribution of the mass of the cells in a maple leaf model, the initial mass of cells gradually decreases from veins to boundaries.

4.3. Permeation and water content

The protoplast layer of plant cells can be regarded as a permselective membrane, water molecules can move freely in and out of it, which is known as the permeation effect. Due to the permeation between leaf cells, the concentration of cytosol increases when dehydration occurs, after that, water molecules enter the cell from outside to maintain the balance of cytosol concentration. By using the Laplacian operator of permeation which is improved by Jeong [11], the variations of the water content during the withering and dehydration process can be given as:

$$w^{n+1}=(w^n-w_{loss}\Delta t)(1-\Delta t L_i^n)^{-1} \quad (1)$$

where Δt indicates the iteration time step, w_{loss} denotes the water content lost due to transpiration in unit time, i.e., the dehydration rate. The larger the w_{loss}, the faster the cells lose water. w_{loss} is defined by:

$$w_{loss}=THK \quad (2)$$

where T indicates the ambient temperature, H denotes the ambient humidity and K is the parameter for different leaves.

In Equation 1, L_i represents the Laplace operator of the current cell v_i, which can be obtained from the following equation:

$$L_i^n=\frac{2}{E}\sum_{j}\lambda\frac{b_i w_j^n - b_j w_i^n}{l_{ij}(m_i^n + m_j^n)} \quad ,i=1,2,\ldots,n, j=1,2,\ldots,m$$

where n denotes the number of cells in the leaf model, i.e., the number of vertices in the 3D mesh model G; m is the number of cells in the one-ring neighborhood of v_i; $E=\Sigma l_{ij}$, l_{ij} indicates the rest length of the spring; λ represents the diffusion coefficient of permeation; b_i represents the mass of the cytosolic of cell v_i; w_i^n is the water content of the cell v_i , which can be obtained by: $w_i^n = m_i^n - b_i$.

4.4. Stress analysis

The mechanical properties of plant leaves are closely related to the mechanical behavior of single cells [20]. And the mechanical analysis of the cell is the key component to make the connection between the micro and macro biomechanics of the cells [21]. The macroscopic morphological changes of leaves are the manifestation of many factors in microscopic scales, such as the turgor pressure of each single cell, the penetration effect and the mechanical properties of the cell wall, etc. [22]

In order to obtain accurate and realistic force analysis results, in this article, the movement of each cell v_i in the leaf model G follows the laws of cell mechanics, which is determined by its current mass m_i, spatial coordinate position $\boldsymbol{x}_i$, and the resultant force $\boldsymbol{F}_i$, etc. As shown in Figure 4(b), in addition to defining the elastic force $\boldsymbol{F}e_i$, and the damping force $\boldsymbol{F}d_i$ to maintain the stability of the system, we also define the permeation expansion force $\boldsymbol{F}p_i$ of cells and the system's time-varying external forces $\boldsymbol{F}o_i$ acting on the feature points v_r of the veins. Therefore, the resultant force $\boldsymbol{F}_i$ acting on the cells v_i can be obtained by:

$$\boldsymbol{F}_i=\boldsymbol{F}e_i+\boldsymbol{F}d_i+\boldsymbol{F}p_i+\boldsymbol{F}o_i, i=1,2,\ldots,n$$

where $\boldsymbol{F}e_i=k_s\Sigma(|\boldsymbol{x}_{ij}| - l_{ij})\boldsymbol{x}_{ij}/|\boldsymbol{x}_{ij}|$, $i=1, 2, \ldots, n, j=1, 2, \ldots, m$, which indicates the resultant force of the elastic at v_i from m cells in the one-ring neighborhood of v_i, where k_s denotes the coefficient of elastic; l_{ij} is the initial length of the spring between the cell v_i and v_j; $|\boldsymbol{x}_{ij}|$ is the length of the spring at the current moment. The introduction of system damping force $\boldsymbol{F}d_i$ avoids the problem of system instability caused by excessive oscillation from the movement of the particles. $\boldsymbol{F}d_i$ is given by: $\boldsymbol{F}d_i = k_d\Sigma(\boldsymbol{v}_i - \boldsymbol{v}_i)$, $i=1, 2, \ldots, n, j=1, 2, \ldots, m$, where k_d denotes the damping coefficient, $\boldsymbol{v}_i$ and $\boldsymbol{v}_j$ are the current velocity of the corresponding particle (see Equation 3).

Furthermore, the liquid inside the cell is wrapped by the cell wall and the plasma membrane, generating pressure. The difference between this pressure and the external standard atmospheric pressure is defined as the swelling force. The cell swelling force $\boldsymbol{F}p_i$ acting on the particle v_i is defined as: $\boldsymbol{F}p_i = k_p\Sigma\alpha_{ij}\Delta p_i\boldsymbol{x}_{ij}/|\boldsymbol{x}_{ij}|$, $i=1, 2, \ldots, n, j=1, 2, \ldots, m$, where k_p indicates the coefficient of swelling force; α_{ij} denotes the area of the j-th triangle among the m triangles formed by the particle cell v_i with the m cells in the one-ring neighborhood; ΔP_i is the difference between the internal and external pressure of the particle v_i at the current moment; The direction of the swelling force is as same as the direction where the particle v_j in the neighborhood of the one-ring points to the current particle v_i. Considering that during the leaves withering process, the occurrence of permeation and dehydration shall lead to a decrease in the volume of cells. Set the initial intracellular pressure p_i^0 equals to the extracellular pressure p_{out}, both are standard atmospheric pressure, then p_i can be updated iteratively by: $p_i^{n+1}=p_i^n - (E_v w_{loss}) / (w_i^n \Delta t)$, $i=1,2,\ldots,n$, then ΔP_i can be updated by: $\Delta p_i^{n+1}=p_{out} - p_i^{n+1}$, and the elastic modulus E_v can be obtained by $E_v = c / (1-2\mu)$. Where c denotes the cell constant; μ indicates the Poisson ' s ratio; w_i^n represents the water content of the cell v_i at the current moment (in Equation 1) and w_{loss} is the dehydration rate (in Equation 2).

In this article, the system's time-varying external force defined at the feature point v_r of the vein is given as: $\boldsymbol{fout}_r^{n+1}= \boldsymbol{fout}_r^n + \boldsymbol{k}_r\Delta t$, where $\boldsymbol{k}_r$ is a vector of adjustment coefficient. Then the resultant force of the system's time-varying external forces acting on cell v_i at each feature point v_r can be obtained by: $\boldsymbol{F}_{Oi}=\Sigma\boldsymbol{fout}_r^{n+1} e^{-K_r gd_{ir}}$, $i=1, 2, \ldots, n, r=1, 2, \ldots, q$, where q is the number of the feature points of the veins; gd_{ir} denotes the discrete geodesic distance from the current particle v_i to the feature point of vein v_r; K_r indicates the corresponding adjustment coefficient, which controls the influence degree of each feature point on the cell v_i.

4.5. Numerical solution

Considering that the forward Euler method has low complexity, but with a restricted time step. The iterative process of this method shall collapse if the time step exceeds the critical value, which makes the method less stable. On the contrary, the backward Euler method has greater stability, but the computational complexity is higher.

Combining the above analysis, in this article, we choose a compromise between the above two methods by solving the motion equation of the leaves' dehydration deformation iteratively via the implicit midpoint method [23]. The improved formulas for the velocity and displacement of the cells v_i are as follows:

	Maple leaves	Poplar leaves	Tilia leaves	Ivy leaves	Willow leaves	Grape leaves
Mass[$m_{\min}$, $m_{\max}$]	[0.70, 1.50]	[0.75, 1.55]	[0.85, 1.65]	[0.8, 1.0]	[0.75, 1.55]	[0.80, 1.50]
Diffusion coefficient λ	0.1	0.1	0.1	0.1	0.1	0.1
Temperature T	20℃	20℃	20℃	20℃	20℃	20℃
Humidity H	50%	50%	50%	50%	50%	50%
Leaf parameter K	2.0×10^{-3}	4.0×10^{-3}	2.0×10^{-3}	4.0×10^{-3}	5.0×10^{-3}	4.0×10^{-3}
Dehydration rate w_{loss}	0.010	0.020	0.010	0.020	0.025	0.020
Spring coefficient k_s	4.0	4.0	4.0	4.0	4.0	4.0
Expansion coefficient kp	1.0	1.0	1.0	1.0	1.0	1.0
Cell constant c	2.0×10^{-4}	2.0×10^{-4}	2.0×10^{-4}	2.0×10^{-4}	2.0×10^{-4}	2.0×10^{-4}
Poisson's ratio μ	0.499	0.499	0.499	0.499	0.499	0.499
Damping coefficient k_d	0.1	0.1	0.1	0.1	0.1	0.1
External force coefficient K_r	1.0	1.0	0.5	1.0	0.8	1.0
Time interval Δt	0.1	0.1	0.1	0.1	0.1	0.1

Table 1. Parameters of the withering deformation

$$\boldsymbol{v}_i^{n+1}=\boldsymbol{v}_i^n+\Delta t\boldsymbol{F}\left(\frac{\boldsymbol{x}_i^{n+1}+\boldsymbol{x}_i^n}{2}\right)/m_i^n, i=1,2,\ldots,n \quad (3)$$

$$\boldsymbol{x}_i^{n+1}=\boldsymbol{x}_i^n+\frac{\Delta t}{2}\left(\boldsymbol{v}_i^{n+1}+\boldsymbol{v}_i^n\right), i=1,2,\ldots,n \quad (4)$$

where m_i^n denotes the mass of v_i at the current moment. Due to the dehydration from cells permeation, the water content of the cells is decreasing with time. As a result, the mass of the cells decreases as the number of iterations increases.

5. Experimental results and analysis

In this article, the experimental environment is a personal computer with Intel(R) Core(TM) i3-4160 CPU, Intel(R) HD Graphics 4400 GPU, 32GB of memory, 64-bit Windows operating system, and with Microsoft Visual Studio 2010 C++ and OpenGL as the environment of programming language. Under this condition, we have constructed the primary veins and simulated the wilting deformation of 6 species of plant leaves, including maple, poplar, tilia, willow, ivy and grape.

Overall, the leaf wilting deformation simulation process can be decomposed into two parts: wrinkle deformation and curl deformation. Upon the basis of the mass-spring system, the result of wrinkle deformation is determined by cell swelling force generated by the permeation of cellular dehydration, and the curl deformation result depends on the time-varying external force defined at the feature points of each vein. The leaves wilting deformation parameters of the experiment are provided in Table 1.

5.1. Veins construction

In this article, we first locate the feature points on the tips of the veins by using the leaf boundary expansion algorithm, and then construct the primary veins of the 3D leaf mesh model with the petiole points based on the discrete geodesic paths. The results of the primary veins we constructed are shown in Figure 6, there are 6 kinds of plant leaves, including poplar, linden, ivy, willow, and grape.

Fig. 6. Veins construction

Obviously, in all the above species of leaves, the feature points of leaf veins can be accurately found, And the location and shape of the primary leaf veins closely matches the ones in the pictures of the real leaves. These results suggest that the boundary expansion algorithm we proposed in this article is well suited to high quality construction of veins

5.2. The effect of deformation

Figure 7 compares the deformation results of the leaves under different forces. The first row of Figure 7 shows the effect of deformation in different leaves without cell swelling force and time-varying external force. The second row shows the effect when leaves are only affected by cell swelling force and without time-varying external force, to compare with the first row, the cell swelling force makes the wrinkling effect of leaves much more pronounced. The third row shows the result of deformation under the influence of both cell swelling force and time-varying external forces. Obviously, compared with the second row, the curling of leaves is much more pronounced under the time-varying external forces.

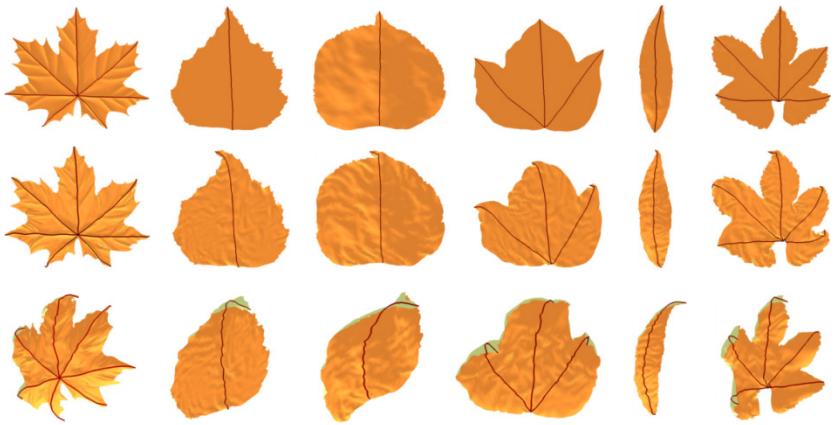

Fig. 7. Effect of wrinkling and curling of leaves under different forces

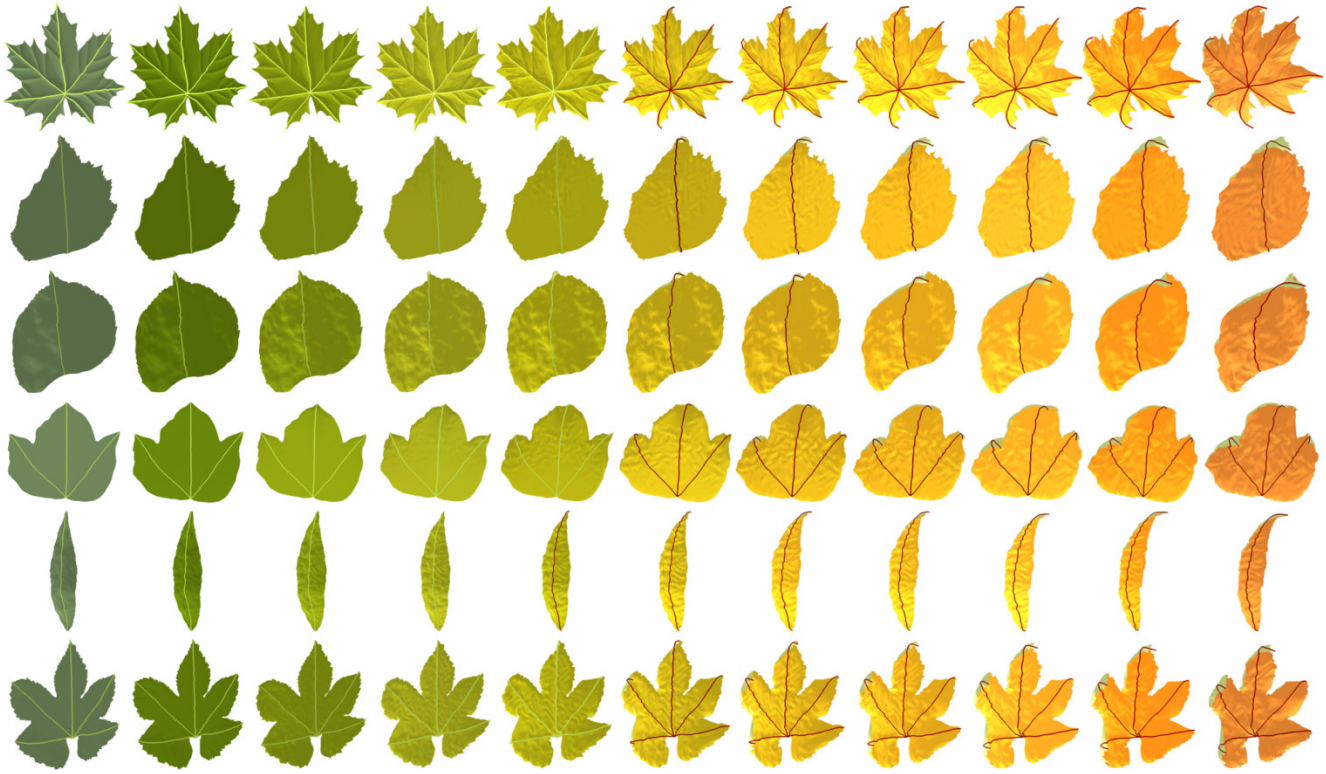

Fig. 8. The middle processes of the wrinkle and curl deformation

The above comparison shows that the cell swelling force we proposed in this article can be effectively used to generate the leaf wrinkle deformation, and the time-varying external forces are effective in producing the leaf curl deformation.

Figure 8 compares the intermediate result of the leaves wrinkle and curl deformation. From left to right, each column shows the intermediate deformation results of different leaves after iterating 0, 10, 20, 30, 40, 50, 60, 70, 80, 90, and 100 times. Obviously, as the iteration increases, the wrinkling and curling during the leaf withering process become more and more obvious, After 100 iterations, it can be seen that realistic leaves withering simulation results can be obtained with our approach.

5.3. Stress change of cells

Take the willow leaf model as an example, Figure 9 shows the change curve of each force magnitude on the cells at the feature points of the veins, vein points, boundaries, and mesophyll during the iterative deformation process, respectively.

As the iteration increases, It can be obviously seen that, firstly, the time-varying external forces defined at the feature points gradually increases, while under the

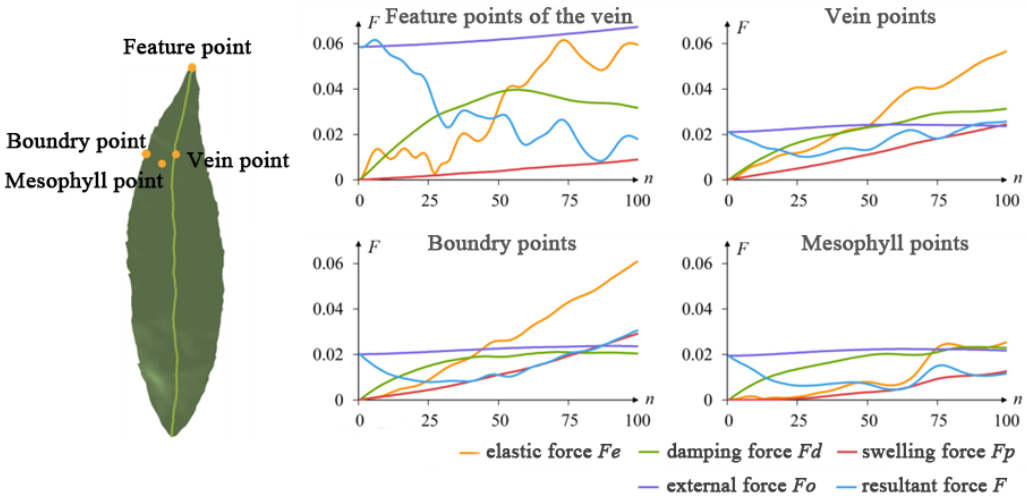

Fig. 9. Stress change curve

Fig. 11. Effect of different water loss rate on the degree of leaf wrinkle

influence of the adjustment coefficient K_r, for cells in other regions, the increase in the external forces transmitted by the feature points of the leaf veins is not obvious.

Secondly, the elastic force increases in a wave-like way, which is caused by the tension or compression of the springs around the cells during the wrinkling process.

Thirdly, the cell swelling force increases steadily, which is because of the continued dehydration of cells, the internal pressure of the cell gradually decreases, and the difference between internal and external pressure increases constantly.

Finally, the damping force is directly proportional to the velocity of cells. The curve of damping force magnitude shows that the velocity of the leaves overall curling deformation is accelerating. But at the feature points of veins, the velocity decreases at the later stage of the iteration, which is because the leaf tips curl inward to make the cells decelerate in a certain direction at the feature points.

5.4. Cell swelling force and water loss rate

When dehydration occurs, the permeation effect of the cells reduces the water content, which makes the leaf curl and deforms under the cell swelling force. A significant factor to measure the water loss of cells is the water loss rate w_{loss}. As the iteration increases, Figure 10 compares the cell swelling force changing curves of a willow leaf's

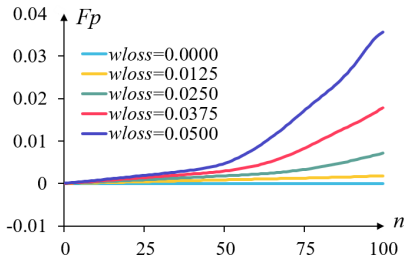

Fig. 10. Effect of water loss rate on cell swelling force

mesophyll cell with different water loss rates w_{loss} during the dehydration process.

Figure 11 compares the wrinkle deformation effect with different water loss rate w_{loss} after 100 iterations. It can be observed that when w_{loss}=0, i.e., when the cell is not dehydrated, there is no swelling force on the cell, and the wrinkle deformation doesn't exist. When w_{loss}>0, which means as the number of iterations increases, the cell will continuously losing water. In this situation, with a larger water loss rate w_{loss}, the rate of the cell swelling force grows faster. As a result, cells have greater swelling force, and the effect of leaf wrinkle deformation is more pronounced.

5.5. The external force and coefficient

Figure 12 compares the effects of leaf curl deformation with different time-varying initial values of external forces

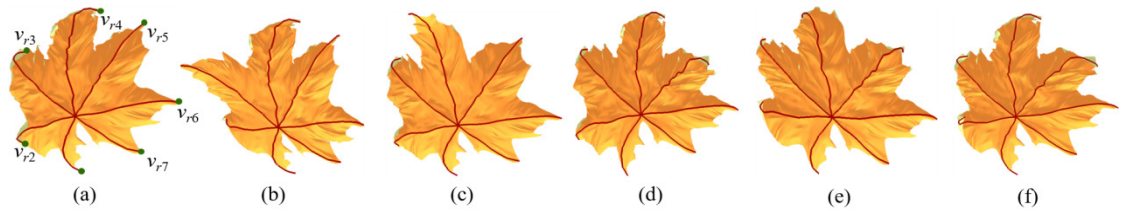

Fig. 12. Deformations of time-varying external force with different initial values

	Figur12(a)	Figur 12(b)	Figur 12(c)	Figur 12(d)	Figur 12(e)	Figur 12(f)
v_{r1}	(0.00 ,0.00, 0.04)	(0.00, 0.00, 0.04)	(-0.01, -0.01, 0.04)	(0.00, 0.00, 0.04)	(0.00, 0.00, 0.04)	(0.00, 0.00, 0.04)
v_{r2}	(0.00, 0.00, 0.04)	(0.00, 0.00, 0.04)	(0.00, 0.00, 0.04)	(0.04, 0.04, 0.04)	(0.00, 0.04, 0.04)	(0.00, 0.04, 0.04)
v_{r3}	(0.01, 0.01, 0.04)	(0.01, 0.01, 0.04)	(0.01, 0.01, 0.04)	(-0.01, -0.01, 0.02)	(0.01, 0.01, 0.04)	(0.01, 0.01, 0.04)
v_{r4}	(0.03, -0.03, 0.03)	(0.00, -0.03, -0.03)	(0.03, -0.03, 0.03)	(0.03, -0.03, 0.03)	(-0.03, -0.03, 0.03)	(-0.03, -0.03, 0.03)
v_{r5}	(-0.02, 0.01, 0.04)	(-0.02, 0.01, 0.04)	(-0.03, -0.03, 0.06)	(-0.02, 0.01, 0.04)	(-0.02, 0.04, 0.04)	(-0.02, -0.03, 0.06)
v_{r6}	(0.00, 0.00, 0.04)	(0.00, 0.00, 0.04)	(0.00, 0.00, 0.04)	(-0.04 ,0.00, 0.06)	(0.00, 0.00, 0.04)	(0.00, 0.00, 0.04)
v_{r7}	(0.00 ,0.00, 0.04)	(0.00, 0.00, 0.04)	(0.00, 0.00, 0.04)	(0.00 ,0.00, 0.04)	(0.00, 0.00, 0.04)	(0.00, 0.00, 0.04)

Table 2. The initial values of the system's time-varying external force corresponding to different leaf deformation effects

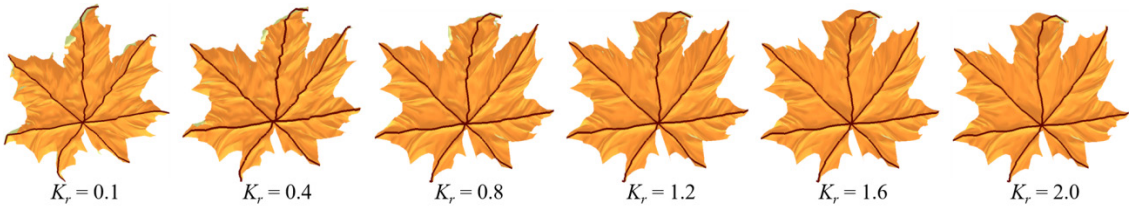

Fig. 13. Effect of external force coefficient K_r on curl deformation

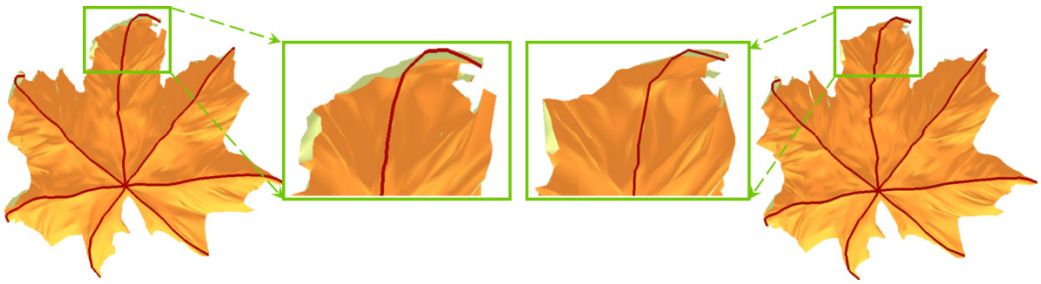

Fig. 14. Comparison of non-uniform distribution with uniform distribution. It shows the deformation effect of leaf with non-uniform mass distribution (a) and with uniform mass (d); (b) and (c) are the corresponding local amplification results.

(including size, direction and adjustment coefficient, etc.). Table 2 provides the details of corresponding values. Obviously, by adjusting the initial values of external forces, the algorithm we proposed in this article is well suited to generate a variety of curl deformation effects.

With the same condition of external forces, different curl deformation effects obtained by setting different external force coefficient K_r can be compared in Figure 13, where K_r is in the range [0, 2]. The comparison shows that when the system time-varying external forces are constant, the extent of curl deformation at the feature points of the leaf veins was proportional to the external force K_r, while the range of curl deformation influenced by the system time-varying external force was inversely proportional to K_r.

5.6. Non-uniform mass distribution

In this article, we define a non-uniform mass distribution, the cells that close to the veins have a larger mass, and the mass of ones that close to the edge and away from the veins are smaller.

Figure 14 compares the effect of the initial mass distribution of leaf cells on the wilting deformation. When the other influencing factors are the same, Figure 14(a) shows the wilting deformation result using our non-uniform mass distribution, and Figure 14(d) shows the result using uniform mass distribution. Figure 14(b) and Figure 14(c) are local amplifications of the corresponding effects.

(a) The deformation result sequence of ivy leaf in reference [12]

(b) The deformation result sequence of ivy leaf with our method

(c) The deformation result sequence of Sycamore leaf in reference [12]

(d) The deformation result sequence of Sycamore leaf with our method

Fig. 15. Comparison of deformation effect between this paper and reference [12]

Obviously, with our non-uniform mass distribution, cells at the edge of the leaf have a higher acceleration, the corresponding degree of curl deformation is more pronounced.

5.7. Compare with related work

Figure 15 shows the comparisons between the results of this article and reference [12]. From these comparisons, the following analyses can be obtained.

Firstly, reference [12] constructs a two-layer model for the veins and a single-layer model for the mesophyll, which has an expensive cost in computation. In order to improve the efficiency, in this article, we adopt single-layer models for both of the veins and mesophylls and use a non-uniform mass distribution to simulate the deformation. As a result, the veins we construct have higher quality and lower computational cost.

Secondly, reference [12] only considers the elastic force and damping force in the simulation process. In contrast, in addition to the above two forces, the algorithm we proposed in this article also introduces the cell swelling force and defines a non-uniform mass distribution. It can therefore be assumed that the wrinkle deformation in this article is much more pronounced.

Finally, it can be seen that the deformation simulations in reference [12] are less natural. In contrast, we introduce the system's time-varying forces in this article to improve the authenticity of the curl deformation.

6. Conclusion

The main goal of the current study was to simulate the deformation of leaves wrinkle and curl due to the dehydration effect. To achieve this goal, we construct a cellular dynamics-based model of leaf wilt and curl deformation, which is based on the mass-spring model defined by cellular dynamics theory and combined with the swelling force describing cell permeation and the time-varying external forces.

In this article, firstly, we propose a boundary expansion algorithm to locate the feature points of the veins and construct the primary veins based on discrete geodetic paths. Secondly, we adopt a mass-spring system of the cells according to the cell dynamics theory, and provide a non-uniform mass distribution to increase the acceleration of the movement of the mass cells in the boundary area. Thirdly, we propose a swelling force of the cells based on permeation theory and water content, and control this force by adjusting the water loss rate. Fourthly, we define the system's time-varying external forces on the veins, and adjust the initial and iterative parameters of the force to simulate the curl deformation of the leaf during the dehydration and wilting process. Finally, the equation of

motion is solved iteratively via the implicit midpoint method to get the simulation results.

Further research in this field would be of great help in improving the authenticity of the simulation. Firstly, in this article, we only consider the geometry simulation of leaves, and simply select color rendering without considering texture synthesis. Thus it would be interesting to introduce the texture mapping and color rendering process into the simulation process. Secondly, considerably more work will need to be done to modify the non-uniform mass distribution interpolation and improve the interpolation formula. Thirdly, It would be interesting to construct two or even multi-level veins to find the best compromise between simulation effect and computational efficiency. Finally, another interesting direction for future work is to take a large number of real leaf texture images with different degrees of wilting and combine them with the geometric deformation model for texture synthesis to further improve the visual effect of leaf wilting deformation from the color and texture perspective.

References

[1] Hong Qin, Boxiang Xiao. Physical model and simulation in virtual reality environment and its application in agricultural information technology [J]. Journal of science and technology. 2018, 36(11): 82-94(in Chinese)

[2] Qinchuan Xin, Yongjiu Dai, Xia Li, et al. A steady-state approximation approach to simulate seasonal leaf dynamics of deciduous broadleaf forests via climate variables [J]. Agricultural & Forest Meteorology, 2018, 249: 44-56

[3] Sunming Hong, R.B. Simpson, G.V.G. Baranoski, et al. Interactive venation based leaf shape modeling [J]. Computer Animation & Virtual Worlds, 2010, 16(3-4): 415-427

[4] D. Kim, J. Kim. Procedural modeling and visualization of multiple leaves [J]. Multimedia Systems, 2016, 23(4): 1-15

[5] A. Runions, M. Tsiantis, P. Prusinkiewicz. A common developmental program can produce diverse leaf shapes [J]. New Phytologist, 2017, 216(2): 401-418

[6] Yulong Han, P. Ronceray, Guoqiang Xu, et al. Cell contraction induces long-ranged stress stiffening in the extracellular matrix [J]. Proceedings of the National Academy of Sciences, 2018, 115(16): 4075-4080

[7] M. Alsweis, O. Deussenn, Jia Liu. Simulation and visualization of adapting venation patterns [J]. Computer Animation and Virtual Worlds, 2017, 28(2): e172

[8] Xiaoyu Chi, Bin Sheng, Yanyun Chen, et al. Modeling of plant leaf morphological change process based on physics [J]. Chinese Journal of Computers, 2009, 32(2): 221-230(in Chinese)

[9] Xiaoyu Chi, Bin Sheng, Yanyun Chen, et al. Simulation of autumn leaves [J]. Journal of Software, 2009, 20(3): 702-712

[10] Hang Xiao, Xi Chen. Modeling and simulation of curled dry leaves [J]. Soft Matter, 2011, 7(22): 10794-10802

[11] S.H. Jeong, S.H. Park, C.H. Kim. Simulation of morphology changes in drying leaves [J]. Computer Graphics Forum, 2013, 32(1): 204-215

[12] Jingjing Wei, Xuehui Liu, Yanyun Chen, et al. Rapid simulation of leaf deformation based on implicit integration [J]. Journal of computer-aided design and graphics, 2015, 27(3): 451-459(in Chinese)

[13] Chuanping Liu, Xiaoyu Guo, Li Wang. Experiment on and simulation of moisture transfer and rolling deformation during leaf drying [J]. Drying technology, 2018, 36(14): 1653-1661

[14] Xuan Huang, Lei Wu, Yinsong Ye. A review on dimensionality reduction techniques [J]. International Journal of Pattern Recognition and Artificial Intelligence, 2019, 33(10):1950017: 1-1950017: 23

[15] Xiang Ying, Caibao Huang, Xuzhou Fu, et al. Parallelizing discrete geodesic algorithms with perfect efficiency [J]. Computer-Aided Design, 2019, 115: 161-171

[16] Xu Zhao, Zongli Jiang. A tangent distance preserving dimensionality reduction algorithm [J]. 2019

[17] [2020-06-20]. https://arxiv.xilesou.top/abs/1902.05373

[18] R.O. Kondareddy, B.A. David. Improved Normalization Approach for Iris Image Classification Using SVM [M]. Innovations in Electronics and Communication Engineering. Springer: Singapore, 2019: 71-79

[19] Shiguang Liu, Dongfang Fan. Computer modeling and simulation of fruit sunscald [J]. International Journal of Image and Graphics, 2015, 15(03): 1550013: 1-1550013: 14

[20] C.R. Munigety. Conformity and stability analysis of a modified spring–mass–damper system dynamics-based car-following model [J]. International Journal of Modern Physics B, 2019, 33(06): 1950025: 1-1950025: 16

[21] A. Geitmann, J.K.E. Ortega. Mechanics and modeling of plant cell growth [J]. trends in plant science, 2009, 14(9):0-478

[22] Zhiyi Fu, Qunying Jiao. Research progress on mechanical models of plant cells [J]. Progress in Mechanics, 2005, 35(3): 404-410(in Chinese)

[23] O. Campas, L. Mahadevan. Shape and dynamics of tip-growing cells [J]. Current Biology, 2009, 19(24): 2102～2107

[24] D. Dinev, Tiantian Liu, L. Kavan. Stabilizing integrators for real-time physics [J]. ACM Transactions on Graphics (TOG), 2018, 37(1): 9: 1-9: 19